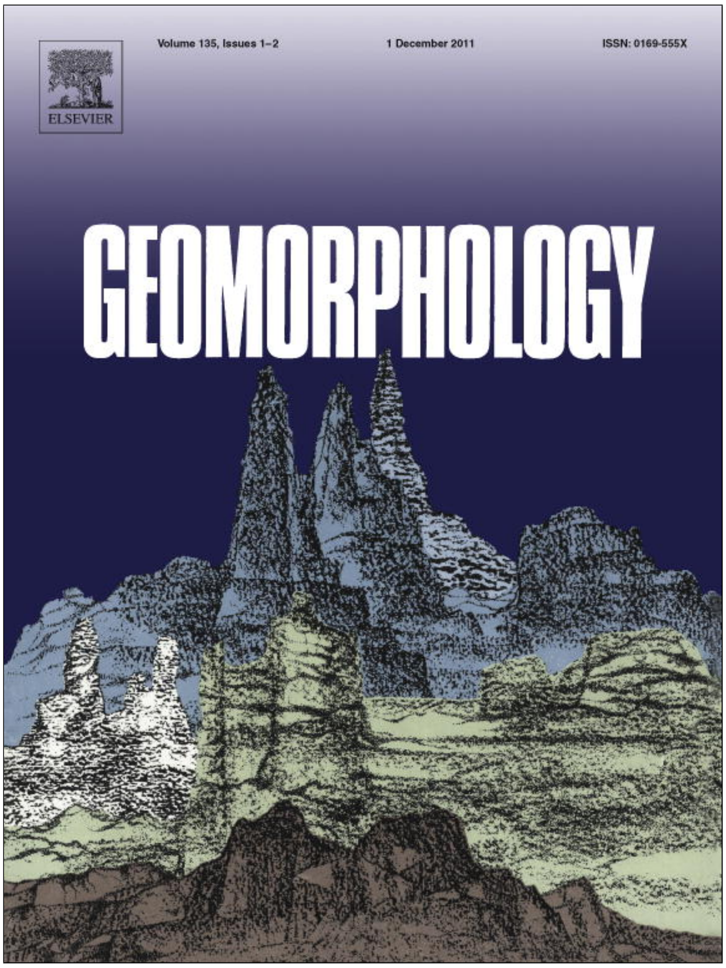
Volume 135, Issues 1–2
1 December 2011
ISSN: 0169-555X
ELSEVIER
GEOMORPHOLOGY

Geomorphology 135 (2011) 167–180

Contents lists available at SciVerse ScienceDirect

Geomorphology

journal homepage: www.elsevier.com/locate/geomorph

Asymmetrical erosion and morphological development of the central Ladakh Range, northern India

Jason M. Dortch [a,*], Lewis A. Owen [a], Lindsay M. Schoenbohm [b], Marc W. Caffee [c]

[a] Department of Geology, University of Cincinnati, Cincinnati, OH 45221, USA
[b] Department of Chemical and Physical Sciences, University of Toronto, Mississauga, Canada ON L5L 1C6
[c] Dept of Physics/PRIME Laboratory, Purdue University, West Lafayette, IN 47906, USA

A R T I C L E I N F O

Article history:
Received 29 April 2011
Received in revised form 4 August 2011
Accepted 12 August 2011
Available online 23 August 2011

Keywords:
Catchment wide erosion
Cosmogenics
Ladakh Range
ELA
Swath
Long river profile

A B S T R A C T

Variations in erosion were quantified across the topographically and morphometrically asymmetrical central Ladakh Range in NW India to elucidate erosion and sediment transfer processes across space and time and to gain insight into how mountains erode and evolve. Morphometric analysis and ^{10}Be cosmogenic nuclide analysis of 14 fluvial sediment samples from active channels in six catchments conducted across the mountain range constrains 100 ka timescale erosion rates for catchments on the northern side of the mountain range and are between 56 ± 12 and 74 ± 11 m/Ma, while catchments on the southern side of the mountain range to between 20 ± 3 and 39 ± 8 m/Ma for the last ~300 ka. Maximum elevation from swath analysis across the range shows a strong correlation with the ELAs of 382 contemporary glaciers. The higher erosion rate to the north likely relates to tectonic tilting of the central Ladakh Range and to active rock uplift on the northern side of the range along the Karakoram Fault. Morphometric analysis shows that the maximum and average elevations increase at nearly the same rate on a catchment-scale across the central Ladakh Range, with higher elevation on the northern side. This suggests that greater erosion on the northern side of the range is not keeping pace with rock uplift. Moreover, long-term denudational unloading does not play a significant role in the tectonic tilting of the central Ladakh Range.

1. Introduction

Researchers have hypothesized that erosional unloading can influence rate and style of tectonic deformation (Molnar and England, 1990; Brozovic et al., 1997; Hodges et al., 2001, 2004; Zeitler et al., 2001; Hodges, 2006) but this hypothesis remains controversial and rates of erosion and sediment transfer need to be quantified to help test these models (Broecker and Denton, 1990; Zeitler et al., 2001; Burbank et al., 2003). Yet, few studies have provided data quantifying the erosion rate across a mountain range, partially because of the lack of adequate methods to determine rates on geomorphic timescales (10^0 to 10^6 years). However, the development of terrestrial cosmogenic nuclide (TCN) methods now provides a means to determine the spatial and temporal variation in erosion (Lal and Arnold, 1985; Bierman, 1994; Bierman and Steig, 1996; Granger et al., 1996; Portenga and Bierman, 2011). To provide some of the first data on erosion rates across a high range in the Himalaya and to begin to test tectonic-climate-erosion models, we undertook a study of the central Ladakh Range, located in the Transhimalaya of northern India, using field mapping, remote sensing and ^{10}Be TCNs. The asymmetric morphology of the central Ladakh Range suggests that erosional unloading affects rock uplift on the northern side of the range, but our results indicate otherwise.

The central Ladakh Range is an ideal study area because the mountain range is easily accessible, of moderate size, and has contrasting styles of deformation, unroofing history, and geomorphology on its northern and southern sides (Fig. 1). The Indus-Tsangpo Suture Zone (ITSZ) bounds the range along its southern margin, which is essentially inactive; whereas the more active Karakoram Fault and Shyok Suture Zone (SSZ) bound its northern side (Rex et al., 1988; Dunlap and Wysoczanski, 2002; Kirstein et al., 2006). Based on thermochronology data from zircon and apatite (U–Th/He) and apatite fission-track methods (AFT), Kirstein et al. (2006, 2009) argued that the central Ladakh Range has been tectonically tilted southward, which results in higher elevations on the northern side of the mountain range during the Late Paleogene (Fig. 2; Table 1). Using morphometric analysis of digital elevation models (DEMs), Jamieson et al. (2004) showed that catchments on the southern side of the central Ladakh Range are significantly shorter, narrower, and have a lower mean elevation than the equivalent catchments on the northern side of the range.

In principle, the tectonic tilting should cause enhanced erosion of northern catchments compared to the southern catchments. Moreover,

* Corresponding author at: Department of Chemical and Physical Sciences, University of Toronto, Mississauga, 3359 Mississauga Rd. N., Mississauga, Canada ON L5L 1C6. Tel.: +1 905 828 5397; fax: +1 905 828 5425.
E-mail address: jason.dortch@utoronto.ca (J.M. Dortch).

0169-555X/$ – see front matter. Crown Copyright © 2011 Published by Elsevier B.V. All rights reserved.
doi:10.1016/j.geomorph.2011.08.014

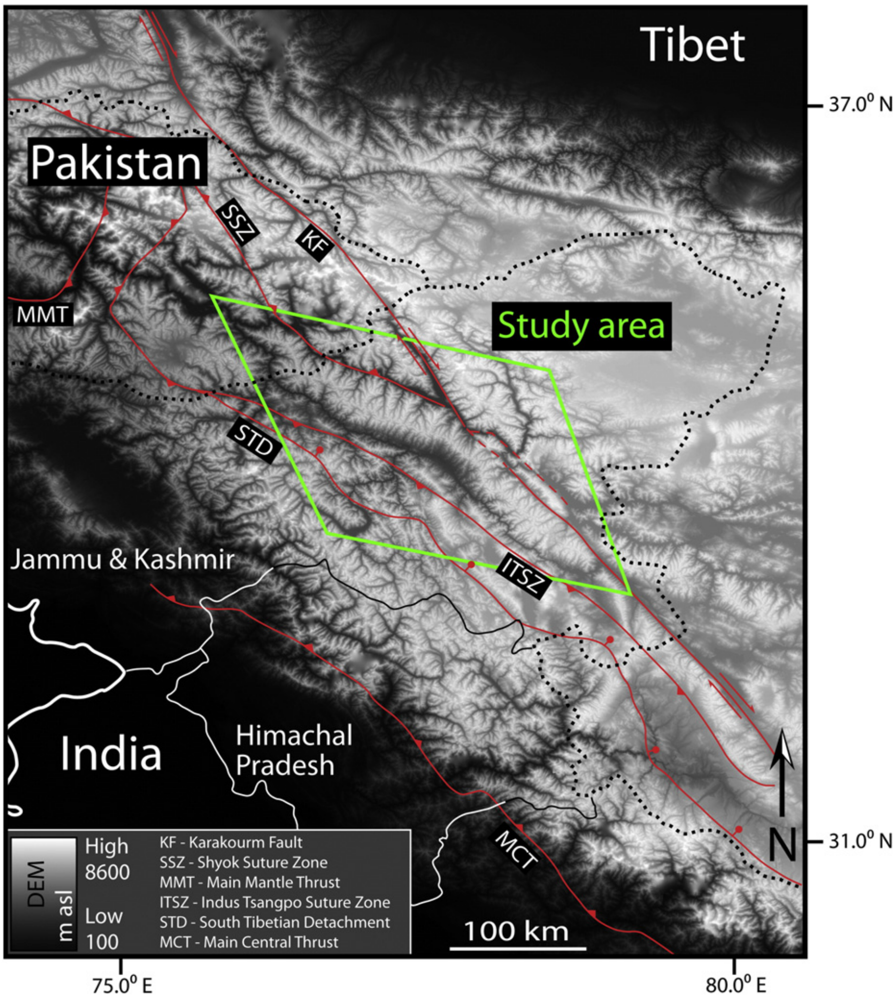

Fig. 1. Shuttle Radar Topography Mission (SRTM) DEM for the NW India Himalaya. The Karakoram Fault (KF) bounds the northeastern edge of the study area. Major faults (from Hodges, 2000) shown in white (red in online version) are (from NW to SW): SSZ — Shyok Suture Zone; ITSZ — Indus-Tsangpo Suture Zone; STD — South Tibetan Detachment; and MCT — Main Central Thrust.

higher erosion on the northern side of the range is expected to create positive feedback between incision, relief, glaciation, and mass movement – inducing denudational unloading and causing the rivers to be in disequilibrium – while the rivers in the southern catchments should aggrade in their lower reaches to advance toward a state of dynamic equilibrium.

In this study, we aim to test these ideas by comparing catchment-wide erosion rates, long valley profiles, equilibrium-line altitude's (ELAs), and basin statistics across the central Ladakh Range using ^{10}Be TCN method, and morphometric analysis. Ultimately, we conclude that asymmetric erosion across the central Ladakh Range is not pervasive enough to influence tectonic processes, which precludes a denudational unloading scenario.

2. Study area background

The Ladakh and adjacent ranges are a consequence of the collision of the Indian and Eurasian continental lithospheric plates starting at ~50 Ma, which resulted in ~2000 km of crustal shortening (Dewey et al., 1989; Johnson, 2002). This collision produced the world's largest and highest orogenic plateau, the Himalayan–Tibetan orogen (Yin and Harrison, 2000; Searle and Richard, 2007). Some of the crustal shortening and thrust and strike-slip faulting are still active (Hodges et al., 2004; Vannay et al., 2004; Bojar et al., 2005).

Located in the Transhimalaya, the Ladakh Range is primarily composed of Cretaceous, continental-arc, plutonic rocks (Searle, 1991). A wide band (≤10 km) of Khardung volcanics comprises the very northern edge of the Ladakh Range (Dunlap et al., 1998).

The inactive ITSZ marks the southern boundary of the Ladakh Range. The Shyok Suture Zone (SSZ) bounds the NW side of the range and is relativity inactive. Rex et al. (1988) suggested that the SSZ was reactivated in the late Tertiary, calling it the Main Karakoram Thrust. The active Karakoram Fault, principally a dextral strike-slip fault, bounds the northeastern side of the range. The Karakoram Fault is a >750–km-long, continental-scale structure that has offset the Indus River ~150 km; however, the evolution and displacement rate along the fault remain hotly debated (Searle et al., 1998; Searle and Owen, 1999; Brown et al., 2002, 2005; Chevalier et al., 2005; Searle and Richard, 2007; Robinson, 2009a,b). Dunlap et al. (1998) showed two periods of oblique, transpressional motion along the Karakoram Fault from 7 to 8 Ma and from 13 to 17 Ma using ^{40}Ar/^{39}Ar methods. Apatite (U–Th/He) and apatite fission-track thermochronometers have yielded Oligocene to Pliocene ages, with progressively younger ages northward across the central Ladakh Range (Choubey, 1987; Sorkhabi et al., 1994; Clift et al., 2002; Schlup et al., 2003; Kirstein et al., 2006, 2009). Based on amphibole thermobarometry data, Kirstein (2011) suggested that rapid cooling (exhumation rate at 0.4 km/Ma) occurred by ~29 Ma on the southern margin and ~22 Ma in the middle of the central Ladakh Range. The most recent phase of exhumation (0.43–0.65 km/Ma) occurred on the northern side of the range since 1517 Ma with the removal of >4 km of material since ~7 Ma (Kirstein, 2011).

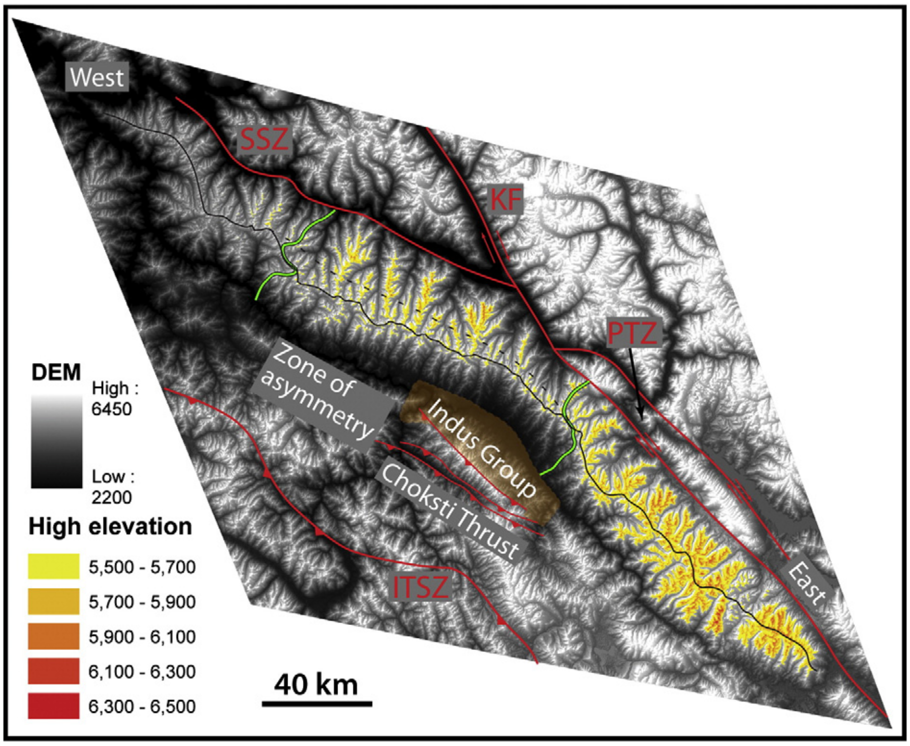

Fig. 2. SRTM DEM highlighting the unequal distribution of high elevation across the central Ladakh Range. The asymmetric central Ladakh Range is marked by thick white lines edged by black lines (green in online version) and Pangong Transpressional Zone (PTZ) marked by black arrow. Location of the Choksti Thrust and Indus Group is taken from Sinclair and Jaffey (2001). Black line (redlines in online version) highlight major faults. See Fig. 1 for location.

Table 1
Area and elevation details by catchment shown in Fig. 7. North and south facing catchment averages are shown in bold.

	Sample catchment area (km^2)	Min elevation (m)	Max elevation (m)	Avg elevation (m)	Standard deviation (m)
North-facing					
1	555	2921	6056	4916	512
2	548	3057	6110	5047	507
3	397	3112	6122	5114	509
4	598	3151	6201	5070	525
5	319	3206	5918	4891	555
6	417	3349	6102	4869	542
Average	**472**	**3133**	**6085**	**4985**	**525**
South-facing					
7	74	2891	5541	4453	594
8	135	2964	5727	4675	585
9	205	2990	5714	4796	550
10	135	3462	5777	4973	458
11	48	3829	5663	4947	428
12	60	3639	5724	4816	490
13	76	3559	5750	4893	492
14	69	3509	5683	4661	537
15	111	3375	5709	4681	555
16	76	3247	5717	4584	593
17	37	3556	5440	4413	426
18	55	3553	5611	4455	504
19	107	3388	5726	4575	618
20	179	3219	5729	4263	651
21	92	3216	5776	4289	686
22	99	3232	5734	4228	682
23	34	3249	5603	4049	549
24	73	3362	5635	4327	568
25	175	3464	5771	4479	566
Average	**97**	**3353**	**5686**	**4556**	**554**

The Ladakh Range contains deeply incised valleys typically with 1–3 km of relative relief and peaks reaching >6 km above sea level (asl). Catchments on the southern side of the central Ladakh Range are choked with thick deposits of alluvium and colluvium (Jamieson et al., 2004). Hobley et al. (2010) and Dortch et al. (2011a) suggested that the lower reaches of rivers in south-facing catchments are aggrading. In contrast, streams in catchments on the northern side of the central Ladakh Range have incised through 150–200 m thick deposits of lacustrine and alluvial sediments that are perched ~1 km above contemporary rivers (Pant et al., 2005; Phartiyal et al., 2005). Based on field observations and ^{10}Be TCN dating of strath terraces, Dortch et al. (2011a) showed that some rivers in north-facing catchments are incising bedrock at mean rates of ~0.6 mm/y over the last 120 ka. Dortch et al. (2011a) also argued that since long-term strath terrace incision rates are equivalent to the rock uplift rates, the northern side of the range is actively uplifting at 0.6 ± 0.1 km/Ma. This is consistent with Kirstein (2011) who suggested exhumation rates of 0.43–0.65 km/Ma on the northern side of the range since 15–17 Ma.

The steep slopes and high elevation (>4.5 km asl) of the Lesser and Greater Himalaya block the majority of summer monsoon circulation (Bookhagen et al., 2005). In spite of this, the monsoon dominates regional moisture transport, precipitation, and the timing of past glacial advances (Owen et al., 2006; Dortch et al., 2009). Sixty years of data from a weather station at the Leh Airport, located within catchment-20, show that the average precipitation in the summer (June–September), winter (December–March), and autumn/spring is ~40, ~30, and ~24 mm, respectively (data repository item DS-1; Weatherbase.com, 2010).

The lacustrine sediment record, former lake levels, and ice core records (Fang, 1991; Gasse et al., 1991, 1996; Shi et al., 2001) show that the south Asian summer moisture has penetrated more than 75 km beyond the present orographic barrier in the past (Bookhagen et al., 2005), which resulted in intensified monsoon precipitation in Ladakh

Table 2
^{10}Be dating and sample details including position, carrier, and ^{10}Be concentrations.

Sample number	Qtz weight (g)	Be carrier weight (g)	Carrier name	Carrier concentration (mg/g)	North latitude (DD)	East longitude (DD)	Altitude (m)	Sample thickness (cm)	^{10}Be/^{9}Be (10^{12})	# of Be-9 atoms (10^{19})	# of Be-10 atoms (10^{6})
BWR-1	23.6845	0.3585	LBCO7	1.354	34.0409	77.8189	4175	1	1.510 ± 0.218	3.24	2.060 ± 0.299
BWR-2	19.0780	0.3485	LBCO8	1.354	34.1878	77.8549	4539	1	1.640 ± 0.060	3.15	2.700 ± 0.099
BWR-3	21.3092	0.3493	LBCO7	1.354	34.3098	77.8365	3387	1	0.992 ± 0.025	3.16	1.470 ± 0.036
BWR-4	21.5997	0.3614	LBCO7	1.354	34.2795	77.7616	4465	1	0.776 ± 0.099	3.27	1.170 ± 0.149
BWR-5	21.0908	0.3571	LBCO7	1.354	34.1587	77.6631	3933	1	1.770 ± 0.065	3.23	2.710 ± 0.099
BWR-6	20.3861	0.3551	LBCO7	1.354	33.9404	77.7676	3488	1	1.400 ± 0.063	3.21	2.200 ± 0.101
BWR-7	20.8741	0.3529	LBCO7	1.354	34.3040	77.3232	3999	1	1.260 ± 0.037	3.19	1.930 ± 0.056
BWR-8	19.1115	0.3531	LBCO7	1.354	34.3391	77.3531	4744	1	1.200 ± 0.026	3.19	2.000 ± 0.044
BWR-10	23.5665	0.3491	LBCO7	1.354	34.4801	77.4333	4183	1	0.698 ± 0.022	3.16	0.935 ± 0.029
BWR-12	22.1461	0.3537	LBCO7	1.354	34.5089	77.4154	3847	1	0.431 ± 0.017	3.20	0.623 ± 0.025
BWR-14	21.6310	0.3538	LBCO7	1.354	34.2539	77.2889	3449	1	0.861 ± 0.136	3.20	1.270 ± 0.202
BWR-15	16.7930	0.3541	LBCO7	1.354	34.2950	77.8426	3491	1	0.584 ± 0.021	3.20	1.110 ± 0.040
BWR-16	20.4941	0.3552	LBCO7	1.354	34.2846	77.8272	3622	1	0.531 ± 0.075	3.21	0.833 ± 0.118
BWR-17	19.3869	0.3561	LBCO7	1.354	34.5786	77.4579	3233	1	0.471 ± 0.036	3.22	0.783 ± 0.060

during the late Pleistocene (24–29 ka and 34–44 ka) and Holocene (Fang, 1991; Gasse et al., 1991, 1996; Shi et al., 2001). Precipitation increased by ~40–100% and likely resulted in enhanced geomorphic activity such as flooding and mass movement and an increase in erosion and sediment transfer (Gasse et al., 1996; Shi et al., 2001; Bookhagen et al., 2005; Dortch et al., 2009, 2011a,b).

Fort (1983) and Burbank and Fort (1985) were the first to describe the glacial deposits in the central Ladakh Range. Building on these studies, Owen et al. (2006) and Dortch et al. (2010) defined the timing of Quaternary glaciation in the central Ladakh Range using ^{10}Be TCN dating and showed that the most extensive preserved late Pleistocene glacial advances occurred at ~160 ka on the northern side and at marine isotope stage (MIS)-8 on the southern side of the range. Glaciers on the northern side of the central Ladakh Range advanced into the Shyok valley at ~160 ka (Deskit-3 glacial stage) extending ~33 km (Dortch et al., 2010), while glaciers on the southern side only extended ~18 km during MIS-8 (Leh stage; Owen et al., 2006). Subsequent glacial advances were less extensive on both sides of the central Ladakh Range; however, morphostratigraphic correlation showed that advances on the northern side of the mountain range were twice as extensive as those on the southern side, albeit still restricted to their valleys (Owen et al., 2006; Dortch et al., 2010).

3. Methods

3.1. Field methods

Landforms and sediments were identified and mapped in the field using topographic maps generated from 15-m resolution Advanced Spaceborne Thermal Emission and Reflection Radiometer (ASTER) and 3 arc-second (~90 m) Shuttle Radar Topography Mission (SRTM) DEMs (CGIAR-CSI, 2007; NASA, 2007). All catchments were traversed from the crest of the range to the sampling locations.

We used ^{10}Be TCN from quartz-rich sands located in active river channels to help determine catchment-wide erosion rates. Approximately 1 kg of sand was collected from the trunk stream of six catchments by wading into the river with a small shovel. Several small scoops were combined in a cloth bag from the active channel. Sediment was sieved between 1 mm and 250 μm in size. Multiple samples were collected to test for nonproportional sediment contribution from subcatchments (Lal and Arnold, 1985; Granger et al., 1996).

The differing geomorphic characteristics of north- and south-facing catchments necessitated separate sampling strategies to check if different parts of the catchments were eroding at similar rates. For catchments on the southern side of the mountain range, the upper samples were collected downstream of moraines from the most recent glacial advance, the Kar glacial stage of Owen et al. (2006); and the lower samples were collected above areas of significant sediment aggradation. For the northern catchments, the upper samples were collected between moraines form the most recent glacial advance — the morphostratigraphic equivalent of Deshkit-1 glacial stage of Dortch et al. (2010) and the start of major river incision of old landforms; and the lower samples were collected near the downstream end of the catchment before lithology changes to the Khardung Volcanics. All samples were collected within the Ladakh batholith where the entire catchment was composed of diorite.

3.2. ^{10}Be surface exposure dating

Isolation of quartz, chemical separation of Be, and preparation of BeO were undertaken in the geochronology laboratories at the University of Cincinnati following the methods of Kohl and Nishiizumi (1992), described in detail in Dortch et al. (2009, and references therein). Ratios of ^{10}Be/^{9}Be were measured using accelerator mass spectrometry at the Purdue Rare Isotope Measurement Laboratory at Purdue University (Table 2).

3.3. Catchment-wide erosion rates

Catchment-wide erosion determined through cosmogenic nuclide inventories in active river sediments yields integrated catchment incision rates averaged over long geomorphic timescales (Schaller et al., 2001). This method fills the gap between traditional erosion rates determined from measured sediment flux (<100 years; Schaller et al., 2001) and exhumation determined through thermochronometry (~1 Ma erosion or exhumation rates; Spotila et al., 2004).

Sediment volume is proportional to erosion rate in a catchment that is close to steady-state and where all the tributaries contribute to the net sediment transfer. In such a case, spatially averaged erosion or incision rates can be calculated for the catchment upstream of the location where sediment is sampled (Lal and Arnold, 1985; Granger et al., 1996). The nuclide concentration within the eroded sediment is a function of the average erosion rate, cosmic ray attenuation length (~60 cm for granitic rocks), and the nuclide production rate at the average catchment surface elevation (Lal, 1991).

Dissolution of sediment and bedrock, sediment storage, significant mass wasting, and nonproportional contribution from tributaries can affect catchment-wide erosion rates (Lal and Arnold, 1985; Granger et al., 1996). Dissolution of granitic regolith and bedrock is assumed to be minor and does not affect the accuracy of catchment-wide erosion rates determined through ^{10}Be TCN inventories in fluvial sediment. The only evidence of recent mass wasting noted in the field was a minor rock fall of four large blocks ~10 m in length in the upper reaches of catchment-4, which would not affect erosion rates for that catchment.

Production rates for ^{10}Be were determined for the catchment upstream of each sampling location using SRTM DEMs. North- and south-facing catchments and the catchment area upvalley of sampling locations were delineated using ArcGIS 1.1 Hydro software in ArcGIS 9.3 (Fig. 3A). Neutron and fast and slow muon production rates were calculated and summed using MATLAB v. (2009) for each pixel (90 m^2) in the catchment based on the scaling factors of Stone (2000) and a revised sea-level low-latitude production rate of 4.49 ± 0.39 ^{10}Be atoms g/quartz/year and a ^{10}Be half life of 1.36 Ma (Nishiizumi et al., 2007). The production rate was corrected for topographic shielding where for each pixel the surrounding pixels are binned into azimuth increments of 30° and the maximum angle to the horizon is used as a shielding estimate for that bin. The shielding correction is small, as surface area on a catchment scale with horizon angles over ~20° is small. The maximum shielding correction factor for our samples is 16%. The production rate of each pixel is shown in data repository item DS-2 and two examples are provided in Fig. 4. The production rates for all pixels in each catchment were averaged to obtain the spatially average production rate used to calculate catchment-wide erosion rates.

3.4. Morphometric DEM analysis

Topography above 5500 m asl was isolated to gain insight into the spatial extent of the zone of asymmetry and its possible correlation to active faults, solar irradiance, and dominant wind direction (Fig. 2). Maximum, minimum, and average catchment elevations were calculated in ArcGIS 9.3 (Table 1). North–south swath analysis was undertaken in MATLAB v. (2009) to define the topography across the zone of asymmetry in the central Ladakh Range. Six DEM swaths, each 25 km wide, were analyzed. Each swath was aligned to completely encompass one of the six large north-facing catchments and two to three of the smaller south-facing catchments. The swath analysis records the maximum, minimum, and average elevation for each pixel band (90 m by 25 km) perpendicular to the 45–60 km swath length. Because the central Ladakh Range varies in width, the swath length varied accordingly. The six swath profiles across the zone of asymmetry also enable longitudinal topographic variation of the central Ladakh Range to be estimated.

3.5. Longitudinal river profiles

A flow direction raster was calculated in ArcGIS 9.3 for each isolated catchment. Catchment DEMs and flow direction rasters were analyzed in MATLAB v. (2009, using the methods of Wobus et al., 2006) to isolate the trunk stream and create a longitudinal profile using a 20-m vertical interval. Digital elevation model artifacts were removed using a 1000-m moving window. To determine concavity, a linear regression was fit to a log–log plot of slope-area data (Wobus et al., 2006). The steepness index was determined by keeping concavity constant (0.45) to allow intra- and intercomparison between reaches and rivers, respectively (Wobus et al., 2006).

Longitudinal river profiles are divided into geomorphic sections (hillslope, glacially dominated, incision, and aggradation) using field photographs, DEMs, and Google Earth. Individual graphs of long river profiles, steepness, knick zones, and geomorphic sections are available for all 25 catchments in the data repository. Knick zones are mapped onto Fig. 5.

3.6. Equilibrium-line altitudes

From the 25 catchments, we identified and mapped a total of 382 contemporary alpine and cirque glaciers on Landsat ETM+ imagery. Resolution of the imagery was sharpened to 15-m resolution with the panchromatic band (Fig. 5). The glaciers were clipped out of 30-m horizontal and 20-m-vertical resolution ASTER GDEM (available from GDEM, 2010). A raster for each glacier was imported into Read-ArcGrid to calculate the hypsometric integral and to bin elevation areas at 10-m intervals (Nash, 2010). The majority of the glaciers were debris-free except near their snouts where till is actively being deposited. The ELA was calculated using the standard area accumulation ratio (AAR) method and ratio of 0.6 (Porter, 1970; Benn et al., 2005). This method is similar to that used by Burbank and Fort (1985), who used AAR (0.65) to reconstruct ELAs in the Ladakh and Zanskar Ranges. The Himalayan ELA reconstruction of Owen and Benn (2005) showed that AAR ratios typically range between values of 0.6 and 0.65. Error for calculated ELA values is taken as ± 20 m, that is, equivalent to the DEM resolution.

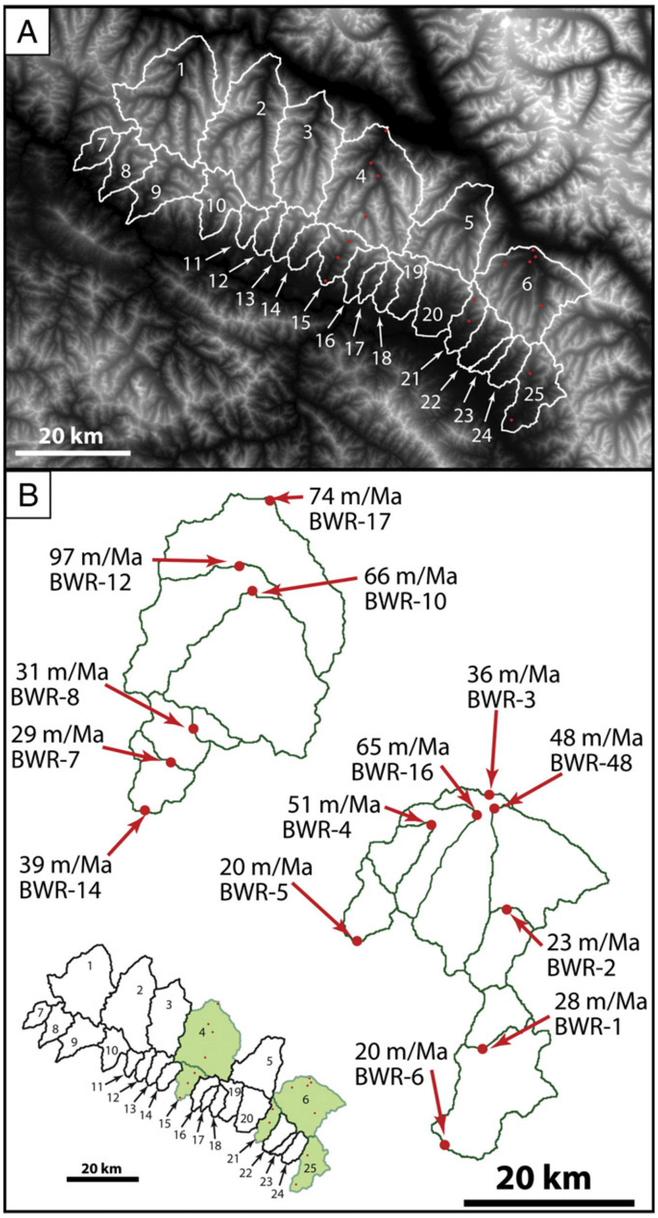

Fig. 3. SRTM DEMs for the central Ladakh Range. (A) Catchments delineated using ArcMap 9.1 and ArcHydro. Sample locations shown by gray dots (red in online version). (B) Subcatchment outlines for each sample with catchment-wide erosion rates. The gray lines (green in online version) delimit each subcatchment area.

4. Catchment descriptions

The major tributaries within the six north-side catchments have well-developed U-shaped valleys containing reduced contemporary

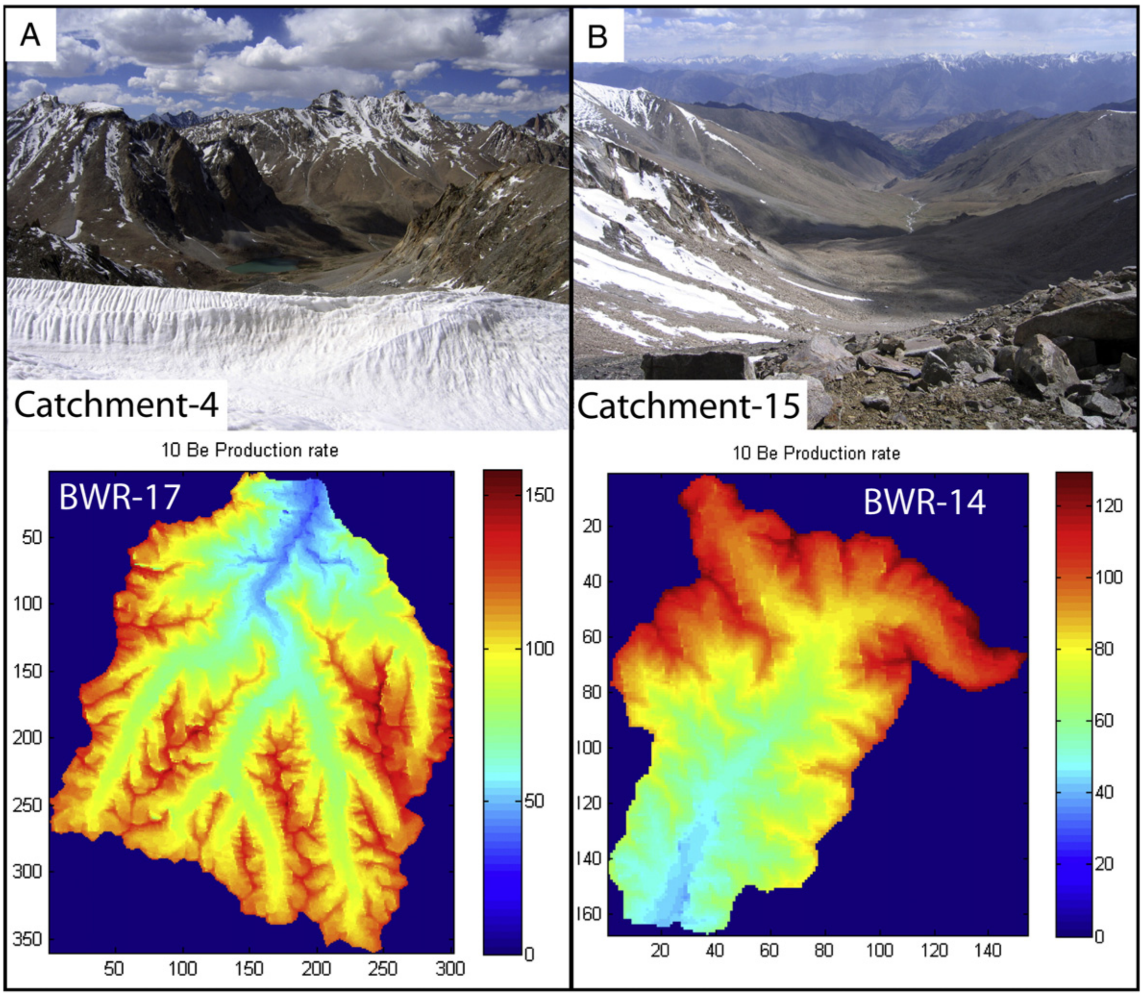

Fig. 4. Views of two typical catchments in the central Ladakh Range and maps showing the calculated ^{10}Be production rates. (A) Catchment-4 and (B) catchment-15 on the northern and southern sides of the central Ladakh Range, respectively, and corresponding ^{10}Be production rate map for each catchment. Note that plot axes are in pixels, thus catchment size is axes number multiplied by 90 m.

glaciers (Figs. 4 and 5). Numerous glaciers are present at the heads of smaller tributaries that are actively eroding; in rare cases, glacially fed sediment cones are present. Regardless of the tributary aspect, all glaciers are sourced on north-facing headwalls. The geomorphology of catchments 4, 5, and 6 (Fig. 6) was mapped in the field by Dortch et al. (2010), who showed that they are dominated by glacial landforms such as moraines, till deposits, roche moutonnées, and glacially polished bedrock (Fig. 6). Extending up from the mouth of the valleys is a 10–20 km zone of deeply incised landforms and bedrock channels. The maximum fluvial incision occurs where the catchments enter the main valley, where 150–200 m thick outcrops of lacustrine and alluvial sediments are perched ~1 km above contemporary rivers (Jamieson et al., 2004; Pant et al., 2005; Phartiyal et al., 2005). Flights of strath terraces up to 120 m tall are present in catchment-4 (Dortch et al., 2011a).

Catchments 7 to 25 on the southern side of the central Ladakh Range only have small tributaries that are dominantly V-shaped valleys, although the uppermost reaches (<10 km) may be moderately developed U-shaped valleys. Small cirque glaciers are present in catchments 7 to 16, 19 to 22, and 24. Erosion is limited for some of these glaciers; yearly visits to catchments 15, 20, 21, and 25 in 2004 to 2008 showed several meters of recent retreat and thinning. While moraines from three glacial stages are present (Owen et al., 2006), the morphology of the catchments is dominated by mass movement and fluvial landforms. Minor fluvial incision of moraine and slope debris occurs for 1–2 km reaches after the Khalling glacial stage deposits of Owen et al. (2006). However, the streams become aggradational and braided downvalley near 4500 m asl. Isolated knobs composed of Ladakh Granodiorite are present in the Indus River valley in-line with south-facing ridges of the central Ladakh Range. They are high topographic points on spurs surrounded by aggrading alluvial and colluvial sediment from the central Ladakh Range and/or buried by large fans advancing north from the Zanskar Range.

5. Results

5.1. Erosion rates

Catchment-wide erosion rates are <100 m/Ma for all catchments in the central Ladakh Range (Fig. 3B; Table 3). Results are discussed in order of catchment number, beginning on the northern side. The samples are described for each from the uppermost sub-catchment to the catchment bottom.

5.1.1. North side: catchment-4

Erosion rates based on samples collected along the main trunk stream in catchment-4 are 66 ± 9 m/Ma (BWR-10), 97 ± 13 m/Ma (BWR-12), and 74 ± 11 m/Ma (BWR-17; Fig. 3B). The increased erosion rate from BWR-10 to BWR-12 suggests that more incision is

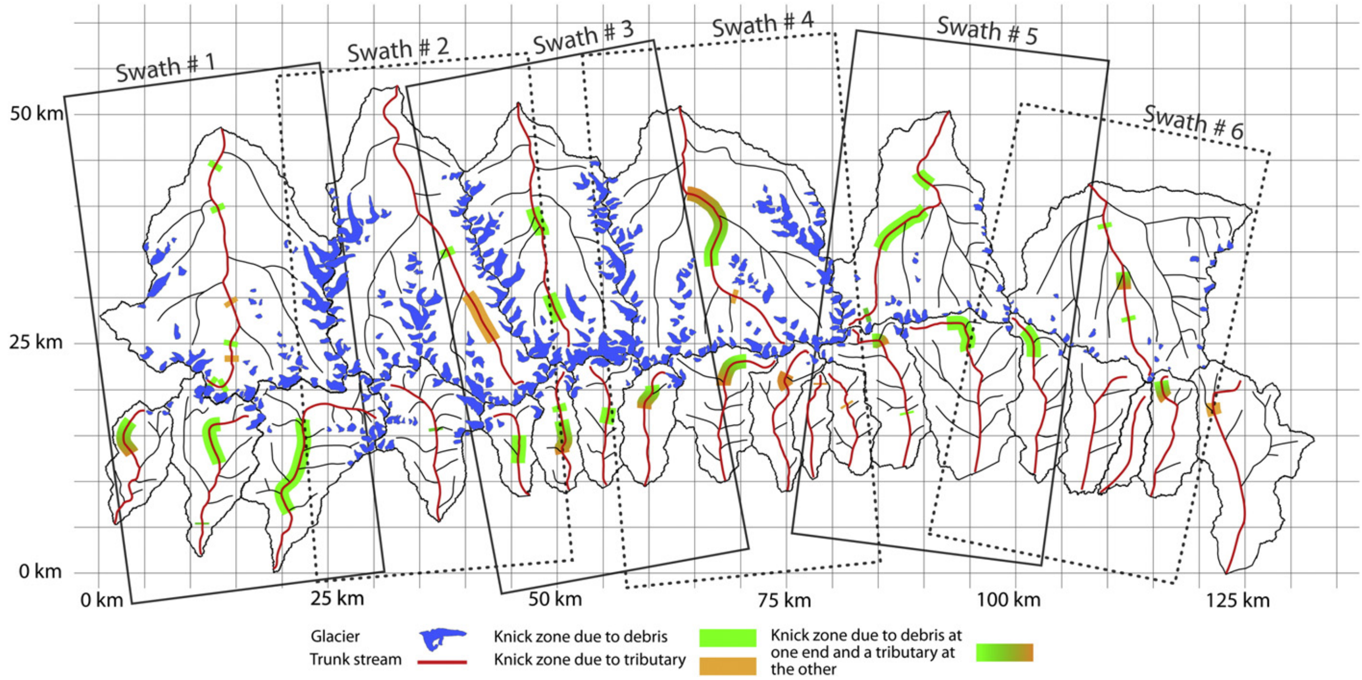

Fig. 5. Catchment outlines showing contemporary glaciers (dark gray; blue in online version), drainage network, and location of swath profiles. Note the J-shape of both trunk streams (thick gray lines; red in online version) and smaller streams (thin black lines) diverging to both the west and the east in south-facing catchments.

occurring in the westernmost tributary. Sample BWR-17, at the end of the catchment, should yield the overall erosion rate for the whole of catchment-4, and indeed the rate is the same within error as the rates obtained from its subcatchments. This indicates that the deeply incised sediments near the end of the catchment are not contributing debris that would artificially increase or lower the erosion rate. We interpret the erosion rate based on sample BWR-17 (74 ± 11 m/Ma) to be the most accurate representation of erosion rate in catchment-4.

5.1.2. North side: catchment-6

Erosion rates based on samples from the westernmost subcatchments in catchment-6 are 51 ± 9 m/Ma (BWR-4) and 65 ± 13 m/Ma (BWR-16), and are within 1 σ error of each other (Fig. 3B). Erosion rates for the easternmost subcatchments range from 23 ± 3 m/Ma (BWR-2) to 48 ± 7 m/Ma (BWR-15). The erosion rate for the subcatchment where BWR-2 was collected is anomalously low compared to the erosion rates from the other three subcatchments. The erosion rate yielded by the lowermost sample in the catchment, BWR-3, at 36 ± 5 m/Ma is lower than the average of the subcatchments, suggesting mixing of modern sediment with sediment from the incised perched lacustrine and colluvial debris, which could have significantly inherited TCNs. Samples BWR-16 and BWR-15 are upstream of the perched debris, within 1 σ error of each other, and should accurately represent the erosion rate of the majority of catchment-6. We therefore exclude BWR-3 and use the average and standard deviation (56 ± 12 m/Ma) of BWR-16 and BWR-15 for an overall erosion rate of catchment-6.

5.1.3. South side: catchment-8

The three samples collected along the trunk stream of catchment-8 yield erosion rates of 31 ± 4 m/Ma (BWR-8), 29 ± 4 m/Ma (BWR-7), and 39 ± 8 m/Ma (BWR-14; Fig. 3B). The erosion rate based on sample BWR-14 is slightly higher but within 1 σ error of erosion rates based on samples from the subcatchments (Table 3). This suggests that erosion throughout the catchment is fairly uniform with no significant reworking of inherited debris. We interpret BWR-14 (39 ± 8 m/Ma) to be the most accurate representation of the erosion and incision of catchment-8.

5.1.4. South side: catchment-21

Only one sample (BWR-5) was collected from catchment-21, from the top of the aggrading section, which is the same geomorphic setting as the other downstream samples collected in the south-facing catchments (Fig. 3B). Sample BWR-5 has an erosion rate of 20 ± 3 m/Ma.

5.1.5. South side: catchment-25

The erosion rate from sample BWR-1 from the upper subcatchment of catchment-25 is 28 ± 6 m/Ma and from BWR-6, at the mouth of the catchment, is 20 ± 3 m/Ma (Fig. 3B). Although these rates are within 1 σ error, the slightly higher erosion rate in the upper reaches of the catchment is expected, as these areas were more recently glaciated. Therefore, sample BWR-6 is the most representative of the overall erosion of catchment-25, with an erosion rate of 20 ± 3 m/Ma.

5.2. Morphometric analysis

Catchments 1 through 6 on the northern side of the central Ladakh Range vary in size from ~320 to ~600 km^2, with an average area of 470 ± 110 km^2 (uncertainty = 1σ), and range in length from 21 to 36 km. Catchments 7 through 25 on the southern side of the central Ladakh Range vary in size from ~34 to ~205 km^2, with an average area of 100 ± 50 km^2. These catchments are 10 to 20 km long. The size of north- and south-facing catchments is distinctly different and does not overlap (Fig. 7, Table 1). More importantly, a positive trend of maximum ($R^2 = 0.86$) and average ($R^2 = 0.39$) and a negative trend of minimum ($R^2 = 0.26$) elevation and catchment size can be seen (Fig. 7). This is reflected also in the significantly greater proportion of the landscape above 5500 m asl on the northern side of the central Ladakh Range (Fig. 2).

Swath analysis between the Shyok and Indus Rivers showed that base level for the tributary rivers on either side of the central Ladakh Range is similar. The minimum elevation across the range indicates that the divide in the first four swaths is shifted to the south as compared to the last two swaths, which are more symmetrically located in the center of the range profile (Fig. 8). Also, the minimum elevation

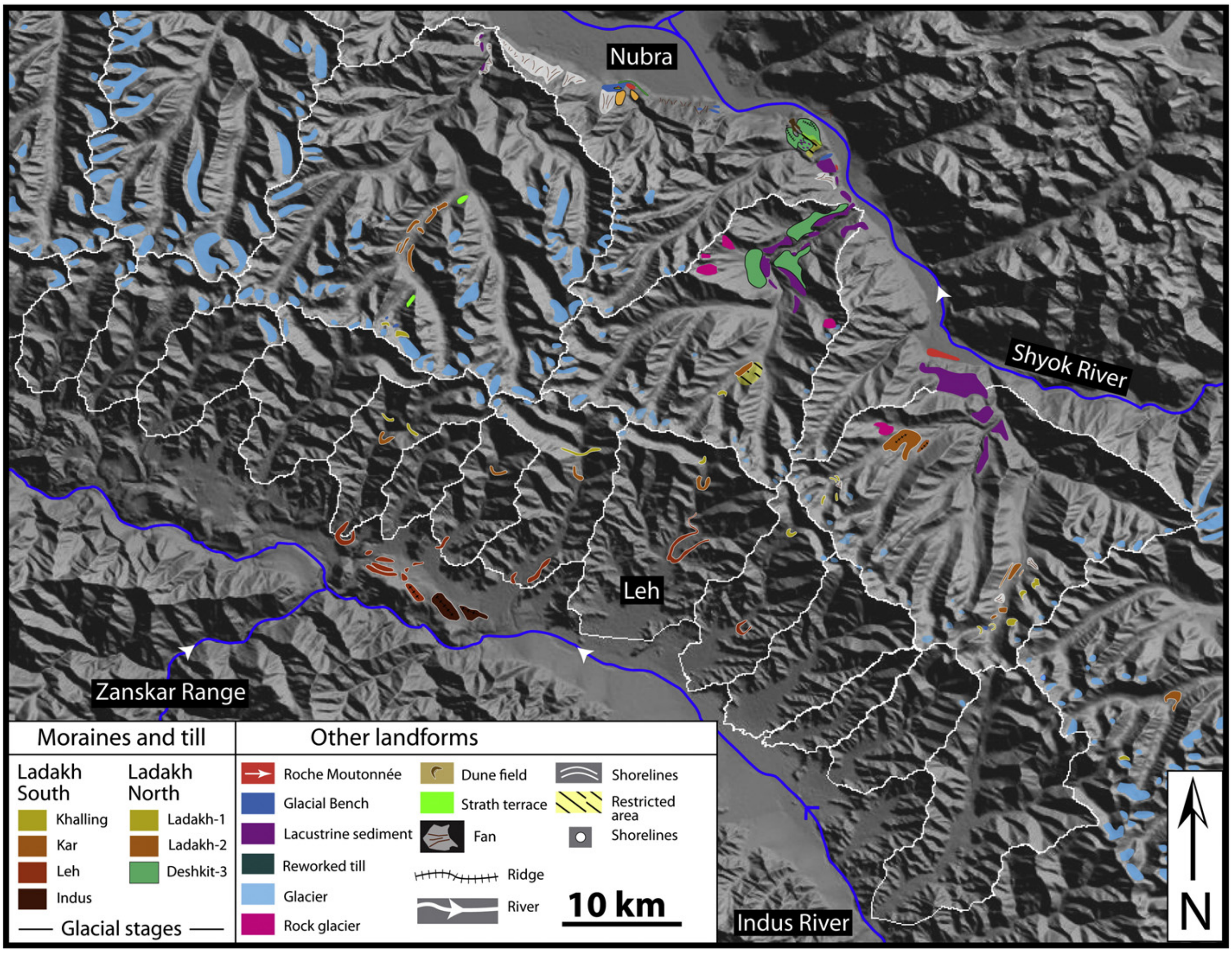

Fig. 6. Geomorphic map of the central Ladakh Range modified from Dortch et al. (2010) with the glacial stages of Owen et al. (2006). The density of glaciers in north-facing catchments is significantly higher than south-facing catchments. Note all contemporary glaciers, including those in south-facing catchments, are sourced on north-facing slopes. See Fig. 3A for location.

profiles from the northern side of the range are stepped and convex-up. The first two profiles on the southern side are convex-up, while the other four are concave-up. The maximum elevation is unusually linear and dips slightly toward the southern side of the range. Relief – the difference between the maximum and minimum elevation profiles – is approximately twice as great (~2 km) on the northern side as on the southern side (~1 km). Average elevation remains high from the divide northward, and then dips down near the Karakoram Fault.

Table 3
Sample subcatchment statistics, MATLAB, 2009 production rates, and resulting erosion rates. Erosion rates and error are shown in bold.

Sample	Corresponding catchment	Sample catchment area (m^2)	Min elevation (m)	Max elevation (m)	Avg elevation (m)	Standard deviation (m)	MATLAB ^{10}Be P-rate	^{10}Be P-error	^{10}Be concentration (10^6)	Attenuation length (m)	Erosion rate (m/Ma)	Error (m/Ma)
BWR-1	25	35.3	4161	5763	5066	375	95.4	12.6	2.062 ± 0.299	0.6	**27.76**	**5.5**
BWR-2	6	49.6	4496	5934	5216	290	101.6	13.5	2.700 ± 0.099	0.6	**22.54**	**3.1**
BWR-3	6	415.7	3389	6102	4874	537	88.3	11.7	1.471 ± 0.036	0.6	**36.03**	**4.9**
BWR-4	6	35.1	4432	5772	5156	284	99.6	13.2	1.174 ± 0.149	0.6	**50.90**	**9.3**
BWR-5	21	37.8	3896	5776	4942	432	90.8	12.0	2.712 ± 0.099	0.6	**20.09**	**2.8**
BWR-6	25	174.6	3464	5771	4479	566	73.7	9.8	2.202 ± 0.101	0.6	**20.08**	**2.8**
BWR-7	15	62.9	3972	5709	5012	367	93.9	12.4	1.929 ± 0.056	0.6	**29.20**	**4.0**
BWR-8	15	15.9	4718	5709	5254	220	103.7	13.7	2.001 ± 0.044	0.6	**31.08**	**4.2**
BWR-10	4	249.9	4141	6105	5231	336	102.4	13.6	0.935 ± 0.029	0.6	**65.73**	**8.9**
BWR-12	4	386.5	3810	6105	5184	381	100.6	13.3	0.623 ± 0.025	0.6	**96.89**	**13.4**
BWR-14	15	109.6	3423	5709	4698	541	81.9	10.8	1.275 ± 0.202	0.6	**38.53**	**8.0**
BWR-15	6	398.7	3473	6102	4913	509	89.5	11.9	1.115 ± 0.040	0.6	**48.17**	**6.6**
BWR-16	6	211.2	3599	5772	4915	468	89.6	11.9	0.833 ± 0.118	0.6	**64.55**	**12.5**
BWR-17	4	593.3	3190	6201	5076	519	96.5	12.8	0.783 ± 0.060	0.6	**73.93**	**11.3**

5.3. Longitudinal river profiles

In general, longitudinal profiles form north-facing catchments are significantly longer than south-facing catchments (Fig. 9). North-facing catchments contain between 2 and 7 knick zones and multiple breaks in steepness from glacial debris (data repository item DS-3). Field mapping and Google Earth imagery showed that there is significant incision at the stream mouth of northern catchments. South-facing catchments contain no or up to 2 knick zones and a maximum of two breaks in steepness from glacial debris. Mapping showed a mix between incision ($n=5$) and aggradation ($n=14$) at the mouth of the valley (Data repository DS-3). Moreover, glacially dominated sections of the long river profiles, recognized by the flat valley bottom, can extend up to 30 km from the divide in north-facing catchments but is restricted to within 8 km from the divide in south-facing catchments.

5.4. ELA reconstructions

The ELAs of the 382 contemporary glaciers are remarkably consistent across the region, with an average of 5455 ± 130 m (Fig. 8). No discernable ELA trend is observable longitudinally across the asymmetric central Ladakh Range. However, a distinct north–south trend is apparent, as ELAs closely follow the distribution of the highest topography and average ~100 m higher on the northern side.

6. Discussion

The north and south sides of the range differ in a number of significant ways, including sediment storage time, erosion rate, glacial versus fluvial erosional dominance, and topography. The primary reason for this may be tilting of the range and the resultant difference in erosion rate. We explore these ideas below.

6.1. Range asymmetry

Cosmogenically determined catchment-wide erosion rates actually reflect an average erosion rate over a period of time from a few hundred to a few hundred thousand years, depending on the rate of erosion. This time period must be longer than climatic cycles that have a significant effect on erosion rates in order to provide average rates that can be compared to each other and be suitable for extrapolating for comparison to thermochronologic data. Climatic cycles of particular importance include periods of enhanced monsoons and glacial cycles (10^3-year timescale).

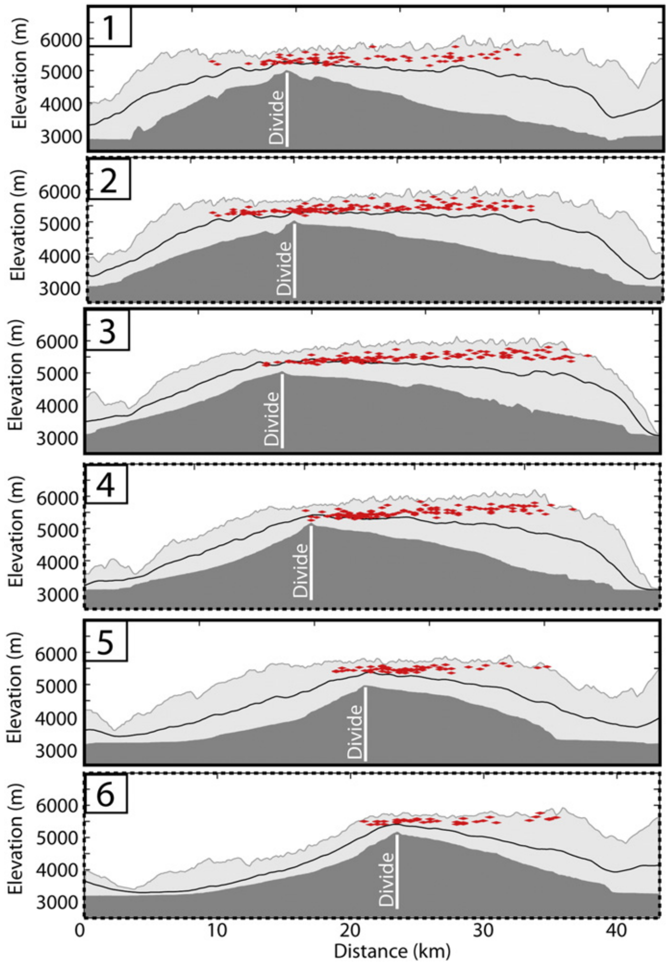

Fig. 8. Swath profiles of the central Ladakh Range coded by boxes. Minimum elevation shown in dark gray and maximum elevation marked by medium gray line. Light gray between maximum and minimum elevations is relief. Average elevation marked by black line. Equilibrium-line elevations for contemporary glaciers are marked by red diamonds. Elevation error (±20 m) and distance error (±0.25 km) do not extent beyond gray diamonds (red in online version).

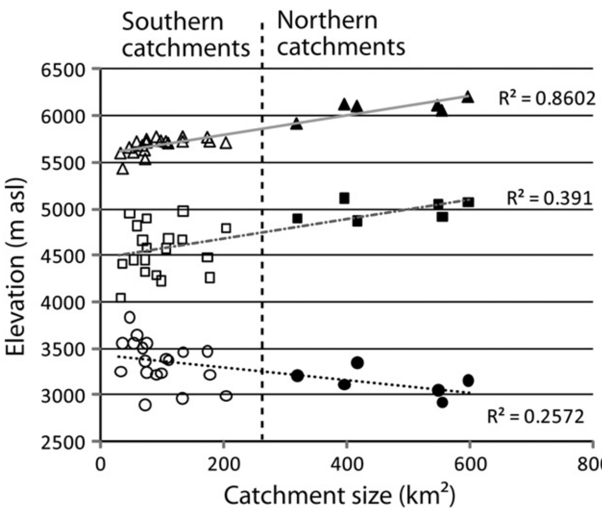

Fig. 7. Plot of maximum (triangles), minimum (circles), and average catchment elevation (squares) versus catchment size in the central Ladakh Range (southern side open markers and northern side closed markers). Trend lines: high elevation — solid light gray line; average elevation — medium ray dash dot line; and minimum elevation — black dotted line. R^2 — square of the correlation coefficient between the regression line and basin data.

Erosion is significantly higher on the north side of the central Ladakh Range, thus the period that catchment-wide erosion rates average should differ across the range. The time period can be estimated by dividing one e-folding depth (or the attenuation length, which is ~60 cm for rock) by the rate of erosion (Lal, 1991). The slow rates of catchment-wide erosion presented here would require ~100 ka (north) and 300 ka (south) to remove a thickness of 60 cm across the entire catchment area. The attenuation length would be longer for sediments, which would increase the time needed to remove sediments. Thus, the erosion rates are integrated over several

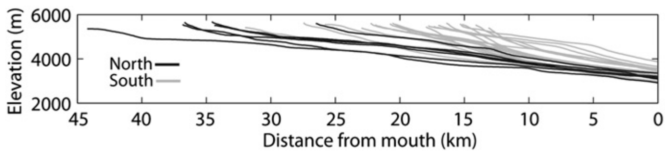

Fig. 9. Long valley profiles of all 25 catchments aligned by the mouth of the valleys.

enhanced monsoon and glaciation/deglaciation cycles and yield a long-term average.

The catchments on the northern side of the central Ladakh Range have catchment-wide erosion rates of between 56 ± 12 m/Ma and 74 ± 11 m/Ma. In contrast, the catchments along the south side of the range are about half those of the northern side, with rates between 20 ± 3 and 39 ± 8 m/Ma (Fig. 3). This suggests that tectonic tilting of the central Ladakh Range and active rock uplift (600 m/Ma; Dortch et al., 2011a) on the northern side of the range has had a significant impact on the rates of erosive geomorphic processes.

Glacial erosion appears to dominate the north side of the range, while fluvial erosion and deposition dominate in the south. Many of the knick zones apparent on the river longitudinal profiles on the northern side of the range correspond to glacial moraines and till. Rivers are restricted to removing glacial debris in much of the catchment and only incise bedrock in the lower reaches (≤10–12 km from valley mouth). Tarns or small proglacial lakes are present in the very uppermost reaches of a few north catchment trunk valleys; however, this could only account for one of the knickzones in each case. Therefore, we suggest that the primary form of erosion is glacial erosion.

The minimum elevation profiles determined from swath analysis of the central Ladakh Range are stepped and convex-up on the northern side. Such profiles are typical of regions dominated by glacial erosion (Brocklehurst and Whipple, 2002, 2004, 2006). The maximum relief is ~1 km higher on the northern side than on the southern side of the range (Figs. 7 and 8). In contrast, the minimum elevation swath analysis showed that catchments 12 to 24 on the southern side are approaching smooth, concave-upward profiles, which suggests that these catchments are dominated by fluvial erosion. The higher maximum and average elevation and greater land surface above 5500 m asl on the northern side of the range likely enhanced accumulation above the ELA, leading to more extensive glacial advances (Dortch et al., 2010) and the development of long, flat sections in the upper portion of long river profiles in the north-facing catchments (MacGregor et al., 2000).

6.2. Glacial headwall backwearing

Glaciers throughout the central Ladakh Range originate exclusively on north-facing slopes, regardless of whether they are on the north or south side of the divide (Figs. 5 and 6). This leads to J-shaped (in planview) trunk streams on the southern side of the range, as glaciers originating on north-facing slopes erode and swing around (Figs. 5 and 6). The ELA distribution with respect to topography (Fig. 8) showed that glaciers are clustered near the divide at the mean topographic elevation. Moreover, ELAs closely mimic the distribution of the highest elevation, which suggests that glacier headwall height controls topography. Similar results were found by Anders et al. (2010) who showed that covariance of peak and cirque elevations support the glacial buzzsaw hypothesis.

Larger, more erosive glaciers on the north side likely increased the rate of glacier headwall backwearing, caused oversteepening of hillslopes, and enhanced mass wasting (Fig. 4). Headward erosion by glaciers appears to be an important force in sculpting the landscape on both sides of the range. In rare cases, glacial headward erosion in the central Ladakh Range has pushed north-side glaciers through the divide, capturing the upper parts of the original south-side catchments and isolating peaks along the former divide north of the modern divide. Increased glacier headwall sapping in northern catchments of the central Ladakh Range, where 81% or 309 of the 382 contemporary glaciers are present, likely caused the southward perturbation in the range divide noted by Jamieson et al. (2004) and the ~100-m decrease in average divide elevation noted by Hobley et al. (2010). Moreover, the higher erosion rates that were measured in the northern catchments are likely caused by cirque headwall sapping. All contemporary glaciers in south-facing catchments ($n = 73$) are of cirque types and are sourced on north-facing walls. This suggests that during times of glacier advance, headwall sapping primarily occurs on north-facing slopes, which would account for the distinctive J-shape of the upper south-facing catchment tributaries.

The asymmetric distribution of relief (Fig. 8) is similar to results from swath analysis by Foster et al. (2010) of the Teton Range, USA. Back tilting along a normal fault created topographic asymmetry, which promoted increased glacial erosion on the eastern side of the Teton Range and ~8 km of erosion-driven migration of the range divide. Similarly, Schoenbohm et al. (2009) suggested that more vigorous glaciation on the eastern side of Muztagh Ata, China, created the amphitheater headwall in the core of the massif and drove the surface trace of the bounding normal fault westward. In both cases, shading caused by topography, precipitation gradient, and redistribution of snow from wind played an important role in promoting glaciation on one side of a range and initiating a positive feedback between topography, glacier accumulation area, glacier size, and erosion rate.

Other studies have similarly documented the importance of glacial headward erosion. Glacial headwall retreat has been suggested to outpace vertical glacial incision, scale with the extent of glaciation, and be the main form of relief production in mountain systems (Whipple et al., 1999; Brocklehurst and Whipple, 2002; Naylor and Gabet, 2007; Spotila, in press). Similar to our study area, in the eastern Kyrgyz Range, Tian Shan, Oskin and Burbank (2005) argued that headwall sapping of north-facing cirques has driven the drainage divide southward at the expense of south-facing valleys at two to three times the rate of vertical incision.

The dominance of north-facing headwalls in our study region is likely the result of increased shading and increased accumulation. Jacobson (2000) measured increased solar radiation and hours of daily sunshine on south-facing slopes in the Leh valley as compared to Nubra valley (Fig. 6; data repository I tem DS-4), which would create a sensible heat gradient across the Ladakh Range, with lower temperatures in the north. The dominant wind direction is to the north as well. The direction of wind has been shown to have a significant effect on the mass-balance of glaciers and their rates of headwall erosion through the transport of wind-blown snow, cross-range precipitation asymmetry, building of cornices, and preferential avalanching (MacGregor et al., 2009; Foster et al., 2010). The reduced insolation received by glaciers on northern slopes in combination with a northward wind direction would significantly promote glaciation on north-facing slopes near the range divide with progressively less precipitation north of the divide. Since Anders et al. (2010) showed that precipitation and cirque elevation are strongly correlated, this would explain the increasing ELAs to the north as well.

From differences in north/south valley length, river long profiles, and the distribution of topography above 5500 m asl, we estimate that the range divide has migrated 3.5 to 11.8 km southward. If divide migration initiated when the range began tilting at ~20 Ma according to Kirstein et al. (2009), headwall backwearing would occur at rates between 0.18 and 0.6 mm/year. This rate is within the range (0.001–5.0 mm/year) of headwall backwearing rates compiled by MacGregor et al. (2009). Thus, the shortening of southern valleys caused by the southward movement of the range divide would have occurred on 10^7-year timescales. Jamieson et al. (2004) suggested that the asymmetric catchment morphology developed on a timescale of 10^6 years (rationale is unclear in their paper). However, a 10^6-year timescale would require headwall backwearing rates (1.8–6.0 mm/year) significantly faster than catchment-wide erosion rates. Moreover, rapid backwearing rates would likely result in debris-covered glaciers, which are not found in the central Ladakh Range.

Viewed on 10^7-year timescales, the rates of catchment-wide erosion would be responsible for ~600 m to 750 m of erosion in the north-facing catchments as compared to 200 to 400 m in the south facing catchments. These rates are modest for the Himalaya, but when eroded volume is considered over the central Ladakh Range, catchments 1 to 6 total 1.7–2.1 × 10^6 m^3 on the north side, while catchments 7 to 25 total 3.7–7.4 × 10^5 m^3 on the south side. We argue that the order of magnitude difference is responsible for the asymmetric morphology of the central part of the range.

6.3. Range tilting

More rapid exhumation of the Indus Group rocks (14 ± 3 Ma AFT age; Sinclair and Jaffey, 2001) compared to the southern side of the central Ladakh Range (30–35 Ma AFT age) led Jamieson et al. (2004) and Kirstein et al. (2006, 2009) to infer a structural relationship in which the Zanskar Range is actively thrusting over the Ladakh Range. However, this hypothesis cannot explain the north–south catchment and divide symmetry of the eastern and western portions of the Ladakh Range or the along-strike gradient from high elevations (east) to lower elevations (west; Fig. 2). Dortch et al. (2011a) noted that strath terraces in the Indus Group rocks demonstrate mean incision rates between 2.0 ± 0.3 and 6.0 ± 0.5 m/Ma for the last ~740 ka. Because fluvial incision over long timescales is a good proxy for rock uplift (Burbank et al., 1996; Leland et al., 1998; Pratt et al., 2002; Willet and Brandon, 2002). Dortch et al. (2011a) suggested that the northern foothills of the Zanskar Range have undergone very little change in base level, thus making thrusting of the Zanskar Range over the Ladakh Range during the last 1 Ma unlikely.

Kirstein (2011) hypothesized that south-directed thrusting of the Karakorum terrane along the Main Karakoram Thrust (MKT) caused the most recent phase of exhumation on the northern side of the Ladakh Range (0.43–0.65 km/Ma since 15–17 Ma). This hypothesis is not supported by contemporary topography. The MKT (equivalent to the SSZ) bounds the northwestern edge of the Ladakh Range, which has lower maximum and average elevations than the central and western portions of the range. Moreover, the morphology of the southern margin of the Ladakh Range does not support the development of the thrust ramp proposed by Kirstein (2011), as the reconstructed drainage divide and location of bedrock knobs clearly demonstrates that the central Ladakh Range was more symmetrical prior to major glaciation.

The spatial topographic pattern suggests an alternative driving force behind the last phase of exhumation of the central Ladakh Range northern side. Maximum elevation of the range is strongly correlated with proximity to the Karakoram Fault. The highest peaks and the majority of surface area above 5500 m asl are located within ~40 km of the Karakoram Fault. Using $^{40}Ar/^{39}Ar$ methods, Dunlap et al. (1998) showed that rocks from mid-crustal depths were exposed in the Pangong Transpersonal Zone (Pangong Range), northern India, because of two periods of oblique thrusting (7–8 and 13–17 Ma) along the Karakoram Fault. The ZFT and AFT thermochronology data indicate that the 3.7 km of exhumation on K2 over the last 4.3 Ma is potentially related to transpressional uplift along the Karakoram Fault (Searle and Phillips, 2007). The Ladakh Range asymmetric zone coincides with a westward bend that moves the range away from the Karakoram Fault and the Pangong Tranpressional Zone (Fig. 2). Major transpression along the Karakorum Fault is consistent in age with the most recent phase of exhumation (0.4–0.6 km/Ma since 15–17 Ma; Kirstein, 2011) on the northern side of the central Ladakh Range. Transpression has also been shown to generate significant uplift along the dextral San Andreas Fault System. Using AHe methods, Spotila et al. (1998) showed that the San Gorgonio block has uplifted at a rate ≥1.5 mm/year over the past few Ma because of transpression along the San Andreas Fault system. We suggest that transpression along the dominantly dextral Karakoram Fault has differentially uplifted the eastern portion and the northern side of the central portion of the Ladakh Range and is responsible for the tilting and subsequent asymmetric morphology in the central portion.

Tilting by transpression would cause subsidence of the southern edge of the central Ladakh Range. Such subsidence is supported by geomorphic observations: the development of bedrock knobs in the Indus River valley, aggradation by streams in southern catchments (data repository DS-3), and the accommodation space provided through subsidence filled by large fans from the Zanskar Range noted by Jamieson et al. (2004). Moreover, Hobley et al. (2010) reported that glacial sediments are stored in the lower reaches of the southern catchments for >500 ka, which is an order of magnitude longer than previously reported storage times in the world. The long storage time renders sediment flushing ineffective. Thus, subsidence of the southern edge of the range would lower base level, causing streams to aggrade and enabling the long-term storage of reworked glacial debris (Fig. 10).

The younger thermochronological ages obtained in the Zanskar Range (AFT ages of Sinclair and Jaffey, 2001) could be explained by either internal deformation of the Zanskar Range along the Choksti Thrust system that parallels the ITSZ. Another explanation may be that exhumation rates are a proxy for erosion (movement of rocks toward the surface), not rock uplift (movement of rocks with respect to the geoid). The metasedimentary rocks that comprise the Zanskar Range are weak and easily eroded. The faster, long-term erosion/exhumation of the Zanskar Range as compared to the southern Ladakh Range would provide the sediment needed to create the large fans that are present in the Indus River valley today.

6.4. Erosional unloading

On both sides of the central Ladakh Range, maximum and mean elevations are positively correlated with catchment size with a similar slope (Fig. 7). Minimum elevation, in contrast, is negatively correlated with catchment size. This suggests that while rivers are responding in the lower reaches to the drop in base level on the northern side of the range by incising and reducing the minimum elevation, the average elevation of the landscape is not being similarly reduced. This is also shown by the swath profiles where the average elevation generally remains high and then drops steeply near the Karakorum Fault. We argue that erosion is not keeping pace with rock uplift. This is confirmed by catchment-wide erosion rates on the northern side of the range that are an order of magnitude slower (60–70 m/Ma) than the rock uplift 600 m/Ma (Dortch et al., 2011a). Thus, we preclude the possibility of long-term denudational unloading from having a significant influence on the tectonic tilting of the range. Moreover, because rock uplift is outpacing erosion and maximum topography follows the conditions of the glacial buzzsaw hypothesis, the average elevation must be increasing and will continue to do so until limited by the ELA as long as the northern side of the range remains tectonically active. Therefore, we suggest that the central Ladakh Range is a transient landscape moving toward a state of equilibrium between topography and glaciation.

7. Conclusions

Erosion rates for catchments along the northern side of the central Ladakh Range are between 56 ± 12 and 74 ± 11 m/Ma, while those for catchments along the southern side of the range vary from 20 ± 3 to 39 ± 8 m/Ma. Rates of erosion in northern catchments are approximately twice as fast as those in southern catchments. Our erosion data imply that differential erosion has contributed to the asymmetrical morphology of the central Ladakh Range and that its tectonic tilting has had a significant impact on the rate of erosive geomorphic processes.

Catchment-wide erosion rates are an order of magnitude slower than the rock uplift rates estimated from strath terrace incision by Dortch et al. (2011a). This suggests that the increased erosion on the northern side of the range is not keeping pace with rock uplift there. Morphometric analysis shows that the maximum and average elevations increase at nearly the same rate with catchment size

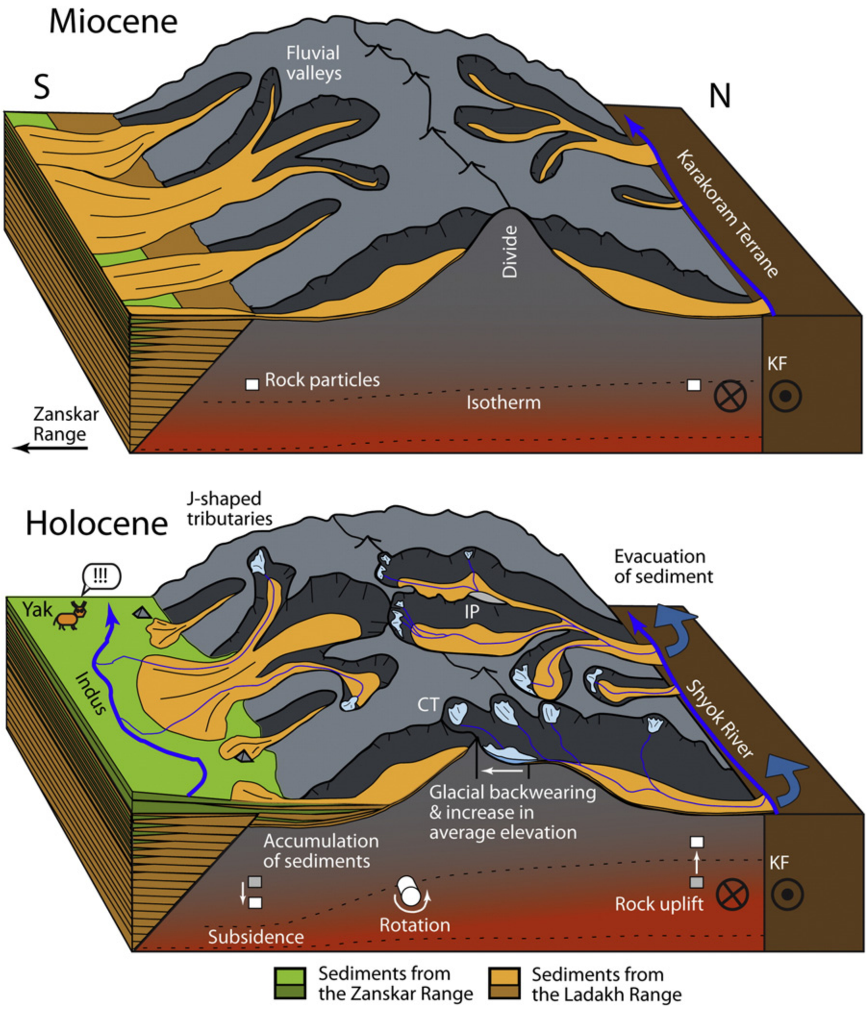

Fig. 10. Schematic representation of the central Ladakh Range illustrating how subsidence and aggradation can create multiple catchments. The Indus River and sediments from the Zanskar Range propagate northward across the Indus valley adjusting to new accommodation space created by the subsidence of the southern edge of the Ladakh Block. Streams in south facing-catchments aggrade to maintain an equilibrium profile and bury the southernmost spurs, shortening valleys, and turning one catchment into several. Linear erosion along the Karakorum Fault (KF) leads to the evacuation and transport of sediments from the northern catchments via the Shyok River. The divide of the central Ladakh Range migrates southward because of enhanced headwall backwearing in the northern catchments, which further shortens valleys and forces southern glaciers to erode parallel of the divide (white arrow indicates offset divide). Greater relief production in northern catchments, isolation of peaks (IP), and capture of tributaries (CT) are caused by enhanced glaciation and headwall backwearing in northern catchments. Uplift of northern margin and subsidence of southern margin likely occur around a pole of rotation that is offset south of the range divide in the central portion of the central Ladakh Range. The pole of rotation is likely (sub)parallel to the Karakoram Fault and bisects the range on an oblique angle: shifted south in the eastern portion of the range and shifted north in the western portion.

with higher elevations on the northern side. This precludes the possibility of long-term denudational unloading from having a significant feedback into the tectonic tilting of the range.

Our study highlights that the synthesis of geomorphic and tectonic data can result in a more complete understanding of the processes that build and shape mountains on various timescales and can prescribe limits to the extent of climate-tectonic feedback. Tectonic processes (transpression) control the tilting of the central Ladakh Range, the gradation in high elevation topography (>5500 m asl), and influence erosion rates. Erosive geomorphic processes are responsible for the asymmetric catchment size, valley spacing/length/width, and incision/deposition of sediments in valleys. Even though erosion is a magnitude of order higher on the northern side of the range, there is no obvious geomorphic feedback into the tectonic system, which sets a minimum limit on the threshold for denudational unloading.

Acknowledgments

Thanks to three anonymous reviewers for their very constructive and positive comments on our manuscript, which helped greatly improved its quality, and to Richard Marston for his very careful edits of our manuscript. JD thanks the Department of Geology, University of Cincinnati for supporting this study as part of his doctoral research; Sigma Xi, the American Alpine Club, and the University Research Counsel of the University of Cincinnati for helping to fund this study; and PRIME Laboratory for measurement of ^{10}Be. LAO and MWC thank the Department of Geology at UC for helping to fund fieldwork and laboratory analysis.

Appendix A. Supplementary data

Supplementary data to this article can be found online at doi:10.1016/j.geomorph.2011.08.014.

References

Anders, A.M., Mitchell, S.G., Tomkin, J.H., 2010. Cirques, peaks, and precipitation patterns in the Swiss Alps: connections among climate, glacial erosion, and topography. Geology 38, 239–242.

Benn, D.I., Owen, L.A., Osmaston, H.A., Seltzer, G.O., Porter, S.C., Mark, B., 2005. Reconstruction of equilibrium-line altitudes for tropical and sub-tropical glaciers. Quaternary International 138–139, 8–21.

Bierman, P., 1994. Using in situ produced cosmogenic isotopes to estimate rates of landscape evolution: a review from the geomorphic perspective. Journal of Geophysical Research 99 13,885-13,896.

Bierman, P., Steig, E.J., 1996. Estimating rates of denudation using cosmogenic isotope abundances in sediment. Earth Surface Processes and Landforms 21, 125–139.

Bojar, A.-V., Fritz, H., Nicolescu, S., Bregar, M., Gupta, R.P., 2005. Timing and mechanisms of central Himalayan exhumation: discriminating between tectonic and erosion processes. Terra Nova 17, 427–433.

Bookhagen, B., Thiede, R.C., Strecker, M.R., 2005. Late Quaternary intensified monsoon phases control landscape evolution in the northwest Himalaya. Geology 33, 149–152.

Brocklehurst, S.H., Whipple, K.X., 2002. Glacial erosion and relief production in the eastern Sierra Nevada, California. Geomorphology 42, 1–24.

Brocklehurst, S.H., Whipple, K.X., 2004. Hypsometry of glaciated landscapes. Earth Surface Processes and Landforms 29, 907–926.

Brocklehurst, S.H., Whipple, K.X., 2006. Assessing the relative efficiency of fluvial and glacial erosion through simulation of fluvial landscapes. Geomorphology 75, 283–299.

Broecker, W.S., Denton, G.H., 1990. What drives glacial cycles? Scientific American 262, 48–56.

Brown, E.T., Bendick, R., Bourles, D.L., Gaur, V., Molnar, P., Raisbeck, G.M., Yiou, F., 2002. Slip rates of the Karakoram Fault, Ladakh, India, determined using cosmic ray exposure dating of debris flows and moraines. Journal of Geophysical Research 107. doi:10.1029/2000JB000100.

Brown, E.T., Molnar, P., Bourlés, D.L., 2005. Comment on "slip-rate measurements on the Karakorum Fault may imply secular variations in fault motion". Science 309, 1326b.

Brozovic, N., Burbank, D.W., Meigs, A.J., 1997. Climatic limits on landscape development in the northwestern Himalaya. Science 276, 571–574.

Burbank, D.W., Fort, M.B., 1985. Bedrock control on glacial limits; examples from the Ladakh and Lanshan Ranges, north-western Himalaya. Journal of Glaciology 31, 143–149.

Burbank, D.W., Anderson, R.S., Brozovic, N., Duncan, C., Fielding, E., Leland, J., Reid, M.R., 1996. Bedrock incision, rock uplift and threshold hillslopes in the northwestern Himalayas. Nature 379, 505–510.

Burbank, D.W., Blythe, A.E., Putkonen, J., Pratt-Sitaula, B., Gabet, E., Oskin, M., Barros, A., Ojha, T.P., 2003. Decoupling of erosion and precipitation in the Himalayas. Nature 426, 652–655.

CGIAR-CSI, 2007. The CGIAR Consortium for Spatial Information. http://srtm.csi.cgiar.org/SELECTION/inputCoord.asp. Accessed on April 2010.

Chevalier, M.-L., Ryerson, F.J., Tapponnier, P., Finkel, R.C., Van Der Woerd, J., Haibing, L., Qing, L., 2005. Slip-rate measurements on the Karakorum fault may imply secular variations in fault motion. Science 307, 411–414.

Choubey, V.M., 1987. Fission track geochronology of the southern part of the Ladakh batholith, Ladakh, northwest Himalaya. Geoscience Journal VIII, 73–80.

Clift, P.D., Carter, A., Krol, M., Kirby, E., 2002. Constraints on India–Eurasia collision in the Arabian Sea region taken from the Indus Group, Ladakh Himalaya, India. In: Clift, P.D., Kroon, D., Craig, J., Gaedicke, C. (Eds.), The Tectonic and Climatic Evolution of the Arabian Sea Region. : Special Publication, 195. Geological Society of London, pp. 97–116.

Dewey, J.F., Cande, S., Pitman, W.C., 1989. Tectonic evolution of the India–Eurasia collision zone. Eclogae Geologicae Helvetiae 82, 717–734.

Dortch, J., Owen, L.A., Haneberg, W.C., Caffee, M.W., Dietsch, C., Kamp, D.U., 2009. Nature and timing of large-landslides in the Himalaya and Transhimalaya of northern India. Quaternary Science Reviews 28, 1037–1054.

Dortch, J.M., Owen, L.A., Caffee, M.W., 2010. Timing and extent of Quaternary glaciation in the Nubra and Shyok valleys, northernmost Ladakh, India. Quaternary Research 74, 132–144.

Dortch, J.M., Owen, L.A., Dietsch, C., Caffee, M.W., Bovard, K., 2011a. Episodic fluvial incision of rivers and rock uplift in the Himalaya and Transhimalaya. Geological Society of London. doi:10.1144/0016-76492009-158.

Dortch, J.M., Owen, L.A., Caffee, M.W., Kamp, D.U., 2011b. Catastrophic partial drainage of Pangong Tso, Ladakh, northern India. Journal of Geomorphology 125, 109–121.

Dunlap, W.J., Wysoczanski, R., 2002. Thermal evidence for early Cretaceous metamorphism in the Shyok suture zone and age of the Khardung volcanic rocks, Ladakh, India. Journal of Asian Earth Sciences 20, 481–490.

Dunlap, W.J., Weinberg, R.F., Searle, M.P., 1998. Karakoram fault zone rocks cool in two phases. Geological Society of London 155, 903–912.

Fang, J.-Q., 1991. Lake evolution during the past 30,000 years in China, and its implications for environmental change. Quaternary Research 36, 37–60.

Fort, M., 1983. Geomorphological observations in the Ladakh area (Himalayas): Quaternary evolution and present dynamics. In: Gupta, V.J. (Ed.), Stratigraphy and Structure of Kashmir and Ladakh Himalaya. Hindustan Publishing Corporation, New Delhi, India, pp. 39–58.

Foster, D., Brocklehurst, S.H., Gawthorpe, R.L., 2010. Glacial-topographic interactions in the Teton Range, Wyoming. Journal of Geophysical Research 115, F01007. doi:10.1029/2008JF001135.

Gasse, F., Arnold, M., Fontes, J.C., Fort, M., Gilbert, E., Huc, A., Bingyan, L., Yuanfang, L., Qing, L., Melleres, F., Van Campo, E., Fubao, W., Qingsong, Z., 1991. A 13,000-year climate record from western Tibet. Nature 353, 742–745.

Gasse, F., Fontes, J.C., Van Campo, E., Wei, K., 1996. Holocene environmental changes in Bangong Co basin (western Tibet). Part 4: discussion and conclusions. Paleogeography, Paleoclimatology, Paleoecology 120, 79–92.

Global Digital Elevation Model (GDEM), 2010. http://www.gdem.aster.ersdac.or.jp/feature.jsp and http://www.ersdac.or.jp/GDEM/E/4.html.

Granger, D.E., Kirchner, J.W., Finkel, R., 1996. Spatially averaged long-term erosion rates measured from *in situ*-produced cosmogenic nuclides in alluvial sediment. Journal of Geology 104, 249–257.

Hobley, D.E.J., Sinclair, H.D., Cowie, P.A., 2010. Process, rates, and time scales of fluvial response in an ancient postglacial landscape of the northwestern Indian Himalaya. Geological Society of America Bulletin 122, 1569–1584.

Hodges, K.V., 2000. Tectonics of the Himalaya and southern Tibet from two perspectives. Geological Society of America Bulletin 112, 324–350.

Hodges, K., 2006. Climate and the evolution of mountains. Scientific American 72–79 August.

Hodges, K.V., Hurtado, J.M., Whipple, K.X., 2001. Southward extrusion of Tibetan crust and its effects on Himalayan tectonics. Tectonics 20, 799–809.

Hodges, K.V., Wobus, C., Ruhl, K., Schildgen, T., Whipple, K.X., 2004. Quaternary deformation, river steepening, and heavy precipitation at the front of the higher Himalayan ranges. Earth and Planetary Science Letters 220, 379–389.

Jacobson, A., 2000. Solar energy measurements of Ladakh, India. Proceedings of the 24th National Renewable Energy Convention 200 of the Solar Energy Society of India, Nov 30–Dec 2, 2000, Mumbai, India.

Jamieson, S.S.R., Sinclair, H.D., Kirstein, L.A., Purves, R.S., 2004. Tectonic forcing of longitudinal valleys in the Himalaya: morphological analysis of the Ladakh batholith, North India. Geomorphology 58, 49–65.

Johnson, M.W.R., 2002. Shortening budgets and the role of continental subduction during the India–Asia collision. Earth Science Reviews 59, 101–123.

Kirstein, L.A., 2011. Thermal evolution and exhumation of the Ladakh batholith, northwest Himalaya, India. Tectonophysics 503, 222–233.

Kirstein, L.A., Sinclair, H., Stuart, F.M., Dobson, K., 2006. Rapid early Miocene exhumation of the Ladakh batholith, western Himalaya. Geologic Society of America 34, 1049–1052.

Kirstein, L.A., Foeken, J.P.T., van der Beek, P., Stuart, F.M., Phillips, R.J., 2009. Cenozoic unroofing history of the Ladakh batholith, western Himalaya, constrained by thermochronology and numerical modeling. Geological Society of London 166, 667–678.

Kohl, C.P., Nishiizumi, K., 1992. Chemical isolation of quartz for measurements of in-situ-produced cosmogenic nuclides. Geochimica et Cosmochimica Acta 56, 3583–3587.

Lal, D., 1991. Cosmic ray labeling of erosion surfaces: *in situ* nuclide production rates and erosion models. Earth and Planetary Science Letters 104, 424–439.

Lal, D., Arnold, J.R., 1985. Tracing quartz through the environment. Proceedings of the Indian Academy of Sciences, Earth and Planetary Sciences 94, 1–5.

Leland, J., Reid, M.R., Burbank, D.W., Finkel, R., Caffee, M.W., 1998. Incision and differential bedrock uplift along the Indus Rver near Nanga Parbat, Pakistan Himalaya, from ^{10}Be and ^{26}Al exposure age dating of bedrock straths. Earth and Planetary Science Letters 154, 93–107.

MacGregor, K.R., Anderson, R.S., Anderson, S.P., Waddington, E.D., 2000. Numerical simulations of glacial-valley longitudinal profile evolution. Geology 28, 1031–1034.

MacGregor, K.R., Anderson, R.S., Waddington, E.D., 2009. Numerical modeling of glacial erosion and headwall processes in alpine valleys. Geomorphology 103, 189–204.

MATLAB v., 2009. Matrix laboratory — the language of technical computing. http://www.mathworks.com/.

Molnar, P., England, P., 1990. Late Cenozoic uplift of mountain ranges and global climate change: chicken or egg? Nature 346, 29–34.

NASA, 2007. National Aeronautics and Space Administration Land Processes Distributed Active Archive Center, Earth Observing Data Gateway. http://edcimswww.cr.usgs.gov/pub/imswelcome/. Accessed on April 2010.

Nash, 2010. ReadArcGrid: histograms elevations read from datasets in ASCII ArcGrid format. Also calculates dimensionless hypsometric curve. http://homepages.uc.edu/~nashdb/. Accessed on April 2010.

Naylor, S., Gabet, E.J., 2007. Valley asymmetry and glacial versus nonglacial erosion in the Bitterroot Range, Montana, USA. Geology 35, 375–378.

Nishiizumi, K., Imamura, M., Caffee, M.W., Southon, J.R., Finkel, R.C., McAninch, J., 2007. Absolute calibration of ^{10}Be AMS standards. Nuclear Instruments & Methods in Physics Research–Beam Interactions with Materials and Atoms 258B, 403–413.

Oskin, M., Burbank, D.W., 2005. Alpine landscape evolution dominated by cirque retreat. Geology 33, 933–936.

Owen, L.A., Benn, D.I., 2005. Equilibrium-line altitudes for the Last Glacial Maximum for the Himalaya and Tibet: an assessment and evaluation of results. Quaternary International 138 (139), 55–78.

Owen, L.A., Caffee, M.W., Bovard, K.R., Finkel, R.C., Sharma, M.C., 2006. Terrestrial cosmogenic nuclide surface exposure dating of the oldest glacial successions in the Himalayan orogen: Ladakh Range, northern India. Geological Society of America Bulletin 118, 383–392.

Pant, R.K., Phadtare, N.R., Chamyal, L.S., Juyal, N., 2005. Quaternary deposits in Ladakh and Karakoram Himalaya: a treasure trove of the paleoclimate records. Current Science 88, 1789–1798.

Phartiyal, B., Sharma, A., Upadhyay, R., Ram-Awatar, Sinha, A.K., 2005. Quaternary geology, tectonics and distribution of palaeo- and present fluvio/glacio lacustrine deposits in Ladakh, NW Indian Himalaya—a study based on field observations. Geomorphology 65, 241–256.

Portenga, E.W., Bierman, P.R., 2011. Understanding Earth's eroding surface with 10Be. GSA Today 21, 4–10.

Porter, S.C., 1970. Quaternary glacial record in Swat Kohistan, west Pakistan. Geological Society of America Bulletin 81, 1421–1446.

Pratt, B., Burbank, D.W., Heimsath, A., Ojha, T., 2002. Impulsive alluviation during early Holocene strengthened Monsoons, central Nepal Himalaya. Geology 30, 911–914.

Rex, A.J., Searle, M.P., Tirrul, R., Crawford, M.B., Prior, D.J., Rex, D.C., Barnicoat, A., 1988. The geochemical and tectonic evolution of the central Karakoram, north Pakistan. Philosophical Transactions of the Royal Society of London 326, 229–255.

Robinson, A.C., 2009a. Geologic offsets across the northern Karakorum fault: implications for its role and terrane correlations in the western Himalayan–Tibetan orogen. Earth and Planetary Science Letters 279, 123–130.

Robinson, A.C., 2009b. Evidence against Quaternary slip on the northern Karakorum fault suggests kinematic reorganization at the western end of the Himalayan–Tibetan orogen. Earth and Planetary Science Letters 286, 158–170.

Schaller, M., von Blanckenburg, F., Hovius, N., Kubik, P.W., 2001. Large-scale erosion rates from *in situ*-produced cosmogenic nuclides in European river sediments. Earth and Planetary Science Letters 188, 441–458.

Schlup, M., Carter, A., Cosca, M., Steck, A., 2003. Exhumation history of eastern Ladakh revealed by ^{40}Ar–^{39}Ar and fission track ages: the Indus River–Tso Morari transect, NW Himalaya. Geological Society of London 160, 385–399.

Schoenbohm, L., Jie, C., Stutz, J., Jie, C., 2009. Glacial erosion, deep exhumation and the development of high topography alng the Kongur detachment, Pamir Mountians, Western China. In: Leech, M.L., Klemperer, S.L., Mooney, W.D. (Eds.), Proceedings for the 25th Himalaya–Karakoram–Tibet Workshop. U.S. Geological Survey, Open-File Report 2010–1099, p. 115.

Searle, M.P., 1991. Geology and Tectonics of the Karakoram Mountains. John Wiley and Sons, Chichester, UK, p. 358.

Searle, M.P., Owen, L.A., 1999. The evolution of the Indus River in relation to topographic uplift, erosion, climate and geology of western Tibet, the Transhimalayan and High Himalayan Ranges. In: Meadows, A., Meadows, P. (Eds.), The Indus River. Oxford University Press, Oxford, UK, pp. 210–230.

Searle, M.P., Phillips, R.J., 2007. Relationships between right-lateral shear along the Karakoram fault and metamorphism, magmatism, exhumation and uplift: evidence from the K2–Gasherbrum–Pangong Ranges, north Pakistan and Ladakh. Journal of the Geological Society 164, 439–450.

Searle, M.P., Richard, J.P., 2007. Relationships between right-lateral shear along the Karakoram fault and metamorphism, magmatism, exhumation and uplift: evidence from the K2-Gasherbrum, Pangong Ranges, north Pakistan and Ladakh. Geological Society of London 164, 439–450.

Searle, M.P., Dewey, J.F., Dunlap, W.J., Strachan, R.A., Weinberg, R.F., 1998. Transpressional tectonics along the Karakoram fault zone, northern Ladakh; constraints on Tibetan extrusion. Geological Society Special Publications, Continental Transpressional and Transtensional Tectonics 135, 307–326.

Shi, Y., Yu, G., Liu, X., Li, B., Yao, T., 2001. Reconstruction of the 30–40 ka BP enhanced Indian monsoon climate based on geological records from the Tibetan Plateau. Paleogeography, Paleoclimatology, Paleoecology 169, 69–83.

Sinclair, H.D., Jaffey, N., 2001. Sedimentology of the Indus group, Ladakh, northern India: implications for the timing of initiation of the palaeo-Indus River. Journal of the Geological Society of London 158, 151–162.

Sorkhabi, R.B., Jain, A.K., Nishimura, S., Itaya, T., Lal, N., Manickavasagam, R.M., Tagami, T., 1994. New age constraints on the cooling and unroofing history of the Trans-Himalayan Ladakh Batholith (Kargil area), N.W. India. Indian Academy of Science Proceedings 103, 83–97.

Spotila, J.A., in press. Glacially-influenced tectonic geomorphology: the impact of the glacial buzz-saw on topography and orogenic systems. In: Owen, L.A. (Ed.), Tectonic Geomorphology, Treatise of Geomorphology. vol. 5. Elesvier, London.

Spotila, J.A., Farley, K.A., Sich, K., 1998. Uplift and erosion of the San Bernardino Mountains associated with transpression along the San Andreas fault, California, as constrained by radiogenic helium thermochronometry. Tectonics 17, 360–378.

Spotila, J.A., Buscher, J.T., Meigs, A., Reiners, P.W., 2004. Long-term glacial erosion of active mountain belts: example of the Chugach/St. Elias Range, Alaska. Geology 32, 501–504.

Stone, J.O., 2000. Air pressure and cosmogenic isotope production. Journal of Geophysical Research 105, 23753–23759.

Vannay, J.-C., Grassmann, B., Rahn, M., Frank, W., Carter, A., Baudraz, V., Cosca, M., 2004. Miocene to Holocene exhumation of metamorphic crustal wedges in the NW Himalaya: evidence for tectonic extrusion coupled to fluvial erosion. Tectonics 23 (TC1014). doi:10.1029/2002TC001429.

Weatherbase.com, 2010. Weather Records and Averages. http://www.weatherbase.com/weather/weather.php3?s=44534&refer=&units=us. Accessed on April 2010.

Whipple, K.X., Kirby, E., Brocklehurst, S.H., 1999. Geomorphic limits to climate induced increases in topographic relief. Nature 401, 39–43.

Willet, S.D., Brandon, M.T., 2002. On steady state in mountain belts. Geology 30, 175–178.

Wobus, C., Whipple, K.X., Kirby, E., Snyder, N., Johnson, J., Spyropolou, K., Crosby, B., Sheehan, D., 2006. Tectonics for topography: procedures, promise, and pitfalls. Special Paper 398, Geological Society of America, Penrose Conference Series, pp. 55–74.

Yin, A., Harrison, T.M., 2000. Geologic evolution of the Himalayan–Tibetan orogen. Annual Reviews of Earth and Planetary Science 28, 211–280.

Zeitler, P.K., Meltzer, A.S., Koons, P.O., Craw, D., Hallet, B., Chamberlin, C.P., Kidd, W.S.F., Park, S.K., Seeber, L., Bishop, M., Shroder, J., 2001. Erosion, Himalayan geodynamics and the geomorphology of metamorphism. Geologic Society of America Today 113, 1443–1455.